Applied Catalysis B: Environmental 91 (2009) 67–72

Contents lists available at ScienceDirect

Applied Catalysis B: Environmental

journal homepage: www.elsevier.com/locate/apcatb

Hydroxide $ZnSn(OH)_6$: A promising new photocatalyst for benzene degradation

Xianliang Fu [a], Xuxu Wang [a,*], Zhengxin Ding [a], Dennis Y.C. Leung [b], Zizhong Zhang [a], Jinlin Long [a], Wenxin Zhang [a], Zhaohui Li [a], Xianzhi Fu [a,*]

[a] Research Institute of Photocatalysis, State Key Laboratory Breeding Base of Photocatalysis, Fuzhou University, Fuzhou, 350002, China
[b] Department of Mechanical Engineering, The University of Hong Kong, Hong Kong, China

ARTICLE INFO

Article history:
Received 22 January 2009
Received in revised form 4 May 2009
Accepted 6 May 2009
Available online 13 May 2009

Keywords:
$ZnSn(OH)_6$
Photocatalysis
Benzene degradation
OH groups

ABSTRACT

Cube-shaped hydroxide $ZnSn(OH)_6$ (ZHS) has been synthesized by a solvothermal process. The obtained sample was characterized by X-ray diffraction (XRD), N_2-sorption (BET surface area), UV–vis diffuse reflectance spectroscopy (DRS), scanning electron microscopy (SEM), transmission electron microscopy (TEM), and Fourier transformation infrared spectroscopy (FTIR). Compared with commercial TiO_2 (Degussa P25), the as-prepared ZHS showed much higher conversion and mineralization of benzene under 254 nm UV irradiation, and no obvious deactivation was observed during the prolonged operation of 50 h. The reasons for the high activity and long-term stability of ZHS will be discussed in terms of the population and the regeneration of surface OH groups.

1. Introduction

Volatile organic compounds (VOCs) are widely used in industrial processes and domestic activities. These extensive uses lead to water and air pollution, particularly indoor air pollution [1]. Among the VOCs, benzene poses the highest cancer risk. One recent report demonstrated that exposure to even 1 ppm of benzene can reduce blood cell counts and cause hematotoxicity in factory workers [2]. Therefore the development of an efficient and mild technology for removing benzene from the ambient environment is absolutely necessary.

Owing to its safety, high reactivity at ambient temperature and low cost, TiO_2-based photocatalytic oxidation has been established as one of the most promising technologies for environment remediation, especially for the decomposition of low concentrations of VOCs [3]. Although a number of VOCs can be readily decomposed to CO_2 and H_2O by TiO_2 photocatalysts [4], the treatment of aromatic compounds like benzene still meets with limited success because of the deactivation caused by the accumulation of the polymerized by-products on the surface [5,6]. Several approaches have been developed to enhance the efficiency and stability of benzene degradation. One is the modification of TiO_2 with noble metals, such as Pt [7], and Rh [8]. Nevertheless the stability of these modified TiO_2 has been concerned about because of the oxidation of noble metal nanoparticles on the TiO_2 surface [8]. In addition, the high cost of precious metal further hinders its application. The other pathway is to optimize the reaction conditions, such as increasing the reaction temperature [7], adding a sufficient amount of H_2O [6] or trace amounts of H_2 into the reaction feed gas [9,10], and introducing a magnetic field into the photochemical reaction system [11]. All of these works greatly improve the photocatalytic efficiency and effectively suppress the sediment of reaction intermediates on the surface of TiO_2. However, it is not easy to realize such a complicated hybrid system for photocatalytic air purification. Therefore, developing a non-TiO_2 photocatalyst with high performance for benzene degradation is indispensable for the application of photocatalysis for the treatment of benzene-polluted air.

As we know, the surface OH groups play an important role in the photocatalytic process, which is ascribed to the fact that they can accept photogenerated holes to form hydroxyl radicals, the principal reactive oxidant in photocatalytic reaction [4]. Since the hydroxide surface is full of OH groups, if it can be excited by UV light, the compound should therefore exhibit high photoactivity, as revealed by the reported $In(OH)_3$ [12] and InOOH [13] photocatalysts. However the photocatalytic activity of hydroxide-based photocatalyst is still rarely explored.

$ZnSn(OH)_6$ (ZHS) is a class of perovskite-structured hydroxide [14]. In the compound the metal atoms are octahedrally coordinated with oxygen atoms to form $Sn(OH)_6$ and $Zn(OH)_6$ polyhedra, and these polyhedra share their "O" corners to build the structural frame-work (Fig. 1). The structure is very similar to that of $In(OH)_3$ [15], which stimulates our interest to investigate its photoactivity. The major applications for ZHS is used as a novel, non-toxic flame-retardant in halogen-containing polymeric materials [16–18] and several

* Corresponding authors. Tel.: +86 591 83779251; fax: +86 591 83779251.
E-mail addresses: xwang@fzu.edu.cn (X. Wang), xzfu@fzu.edu.cn (X. Fu).

0926-3373/$ – see front matter © 2009 Elsevier B.V. All rights reserved.
doi:10.1016/j.apcatb.2009.05.007

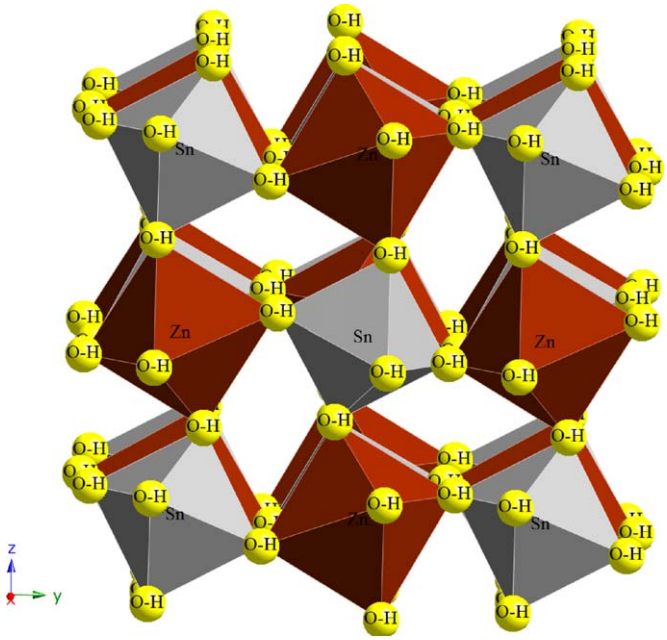

Fig. 1. schematic structure of $ZnSn(OH)_6$.

methods have been developed to prepare ZHS, such as co-precipitation [19,14], sonochemical [14], and hydrothermal reactions [14,20–22]. In addition, our recent research accidentally found that ZHS can be also synthesized by solvothermal method with ethylene glycol as the solvent [23]. In the present paper, ZHS was prepared according to this solvothermal method and its photocatalytic activity for benzene degradation was reported for the first time. The sample, even without the loading of noble metals, shows high photocatalytic activity toward degradation of benzene and no deactivation of the photocatalyst is observed during the prolonged experiment of 50 h. At last, the reason for the high activity and long-term stability of ZHS are discussed in terms of the population and the regeneration of surface OH groups.

2. Experimental

2.1. Preparation of photocatalyst

All of the reagents were analytical grade and used without further purification. In a typical synthesis, 0.70 g $ZnCl_2$ and 1.80 g $SnCl_4{\cdot}5H_2O$ were dissolved in 50 mL of ethylene glycol solvent and stirred at room temperature for 30 min. Then 25 mL of 1.2 M n-butylamine/ethylene glycol solution was added dropwise to the stirred solution. After stirring for 30 min, the obtained white slurry was transferred to a 100 mL autoclave and then maintained at 180 °C for 20 h. The product deposited at the bottom of the autoclave was centrifuged and rinsed thoroughly with deionized water and ethanol several times. Finally, the product was dried in air at 80 °C for 10 h.

2.2. Characterization

X-ray diffraction (XRD) pattern of the sample was collected on a Bruker D8 Advance X-ray diffractometer with Cu Kα radiation (λ = 1.5406 Å). The accelerating voltage and the applied current were 40 kV and 40 mA, respectively. The UV–vis diffuse reflectance spectrum (DRS) was recorded on a Varian Cary 500 Scan UV–vis–NIR spectrometer, where $BaSO_4$ was used as a reference sample. The BET surface area was determined by nitrogen adsorption–desorption, which was measured at 77 K on the Micromeritics ASAP 2020. The morphology of the sample was investigated by field emission scanning electron microscopy (SEM) (XL30ESEM, Philips). Transmission electron microscopy (TEM) and high-resolution TEM (HRTEM) images were obtained by a JEOL model JEM 2010 EX instrument at the accelerating voltage of 200 kV. Fourier transformation infrared (FTIR) spectra on the pellets of the samples were recorded on a Nicolet Nexus 670 FTIR spectrometer at a resolution of 4 cm^{-1}. After the samples were used for the photoreaction, they were taken from the photoreactor, and a fraction of them was diluted with KBr powder. An EPR spectrometer (ESP 300E, Bruker) was used for measurements of the electron paramagnetic resonance (EPR or ESR) signals of photo-induced radicals which were spin-trapped by 5,5-dimethyl-1-pyrroline-N-oxide (DMPO). All freshly prepared solutions were mixed directly before their transfer into a cylindrical quartz cell (length 100 mm; diameter 2 mm). A spot UV-light source of Hamamatsu Co. (LC8) (equipped with a 254 nm filter) was used in situ as a photo-excitation light source, and the ESR spectra were recorded at room temperature.

2.3. Photocatalytic activity measurements

Fig. 2 shows the reaction system and the fixed bed photoreactor used in this study. The photocatalyst (0.45 g, 50–70 mesh) was loaded in a 11-cm-long, 4-mm-diameter reactor surrounded by four 4-W UV lamps with a wavelength centered at 254 nm (Philips, TUV 4W/G4 T5). Benzene diluted in a pure oxygen stream was used as the reactant stream. The flow rate of the reactant mixture was kept at 40 mL min^{-1}. Simultaneous determination of the concen-

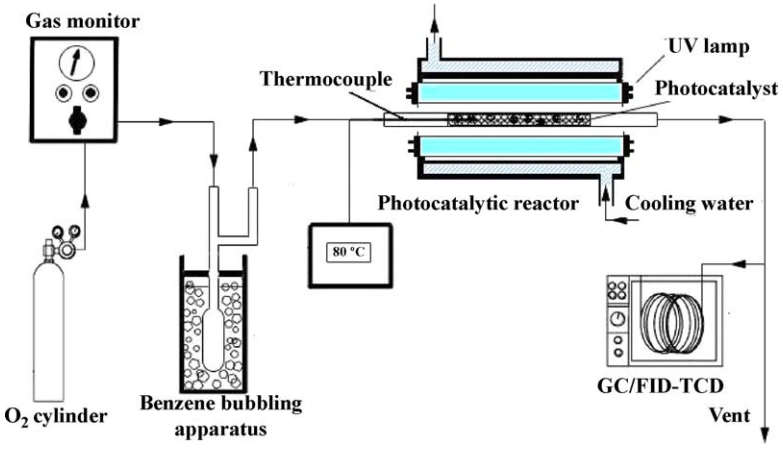

Fig. 2. Schematic diagram of the photocatalytic reaction system.

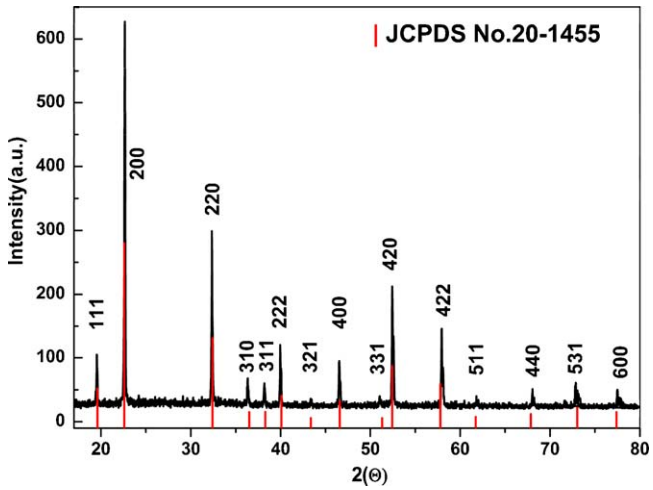

Fig. 3. XRD pattern of the as-prepared $ZnSn(OH)_6$.

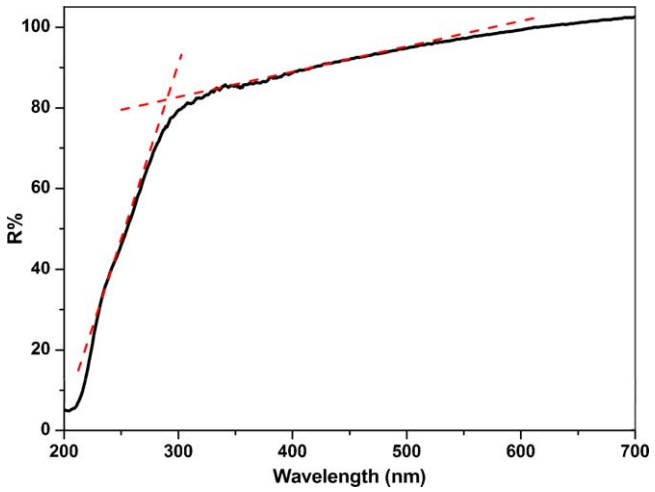

Fig. 4. UV–vis diffuse reflectance spectrum of $ZnSn(OH)_6$.

trations of benzene and carbon dioxide was performed with an online gas chromatograph (HP 6890) equipped with a flame ionization detector, a thermal conductivity detector, and a Porapak R column. During the reaction, the heat generated by the UV lamps was removed by a water jacket around the lamps. The steady reaction temperature was maintained at about 80 °C. Benzene was found to be stable in the catalyst loaded reactor at this temperature in the dark, and no degradation of benzene was observed when it was illuminated in the absence of ZHS. In addition, no CO_2 was detectable when the photocatalyst was illuminated without benzene feed. For comparison, the photocatalytic activity of commercial TiO_2 (Degussa P25) was also tested under the same reaction conditions and with the equal catalyst weight as that employed for ZHS.

3. Results and discussion

The XRD pattern of the as-prepared ZHS is shown in Fig. 3. All of the diffraction peaks can be assigned to the cubic phase of $ZnSn(OH)_6$ (JCPDS 20-1455), with a cell edge of 7.80 Å and space

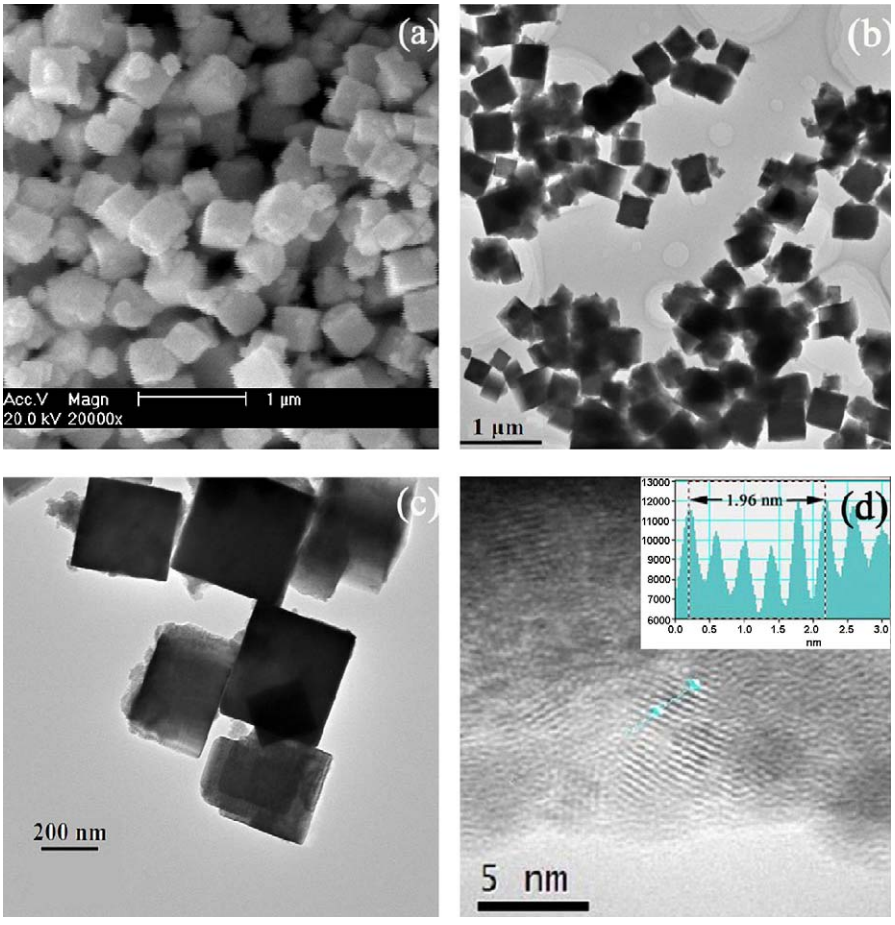

Fig. 5. (a) SEM image; (b) and (c) TEM images; (d) HRTEM image of the as-prepared $ZnSn(OH)_6$.

group *Pn*3*m*. No extra peaks due to the impurity phase are found in the patterns. The BET specific surface area for ZHS is 48 $m^2\ g^{-1}$, which is very close to the value of 50 $m^2\ g^{-1}$ for Degussa P25. The UV–vis diffuse reflectance spectrum of ZHS in Fig. 4 shows an optical absorption threshold at 290 nm, corresponding to a band gap of 4.3 eV.

The overall morphology of ZHS particles was examined using SEM and TEM. As shown in Fig. 5a and b, a large quantity of monodisperse cubes with an edge length of about 350 nm can be observed. It is also clearly seen from Fig. 5b and c that some small nanoparticles are attached to the edge of the nanocubes. An HRTEM image (Fig. 5d) reveals that the lattice fringes of the attached nanoparticles are about 0.39 nm, corresponding to the (2 0 0) d spacing of the cubic phase of the ZHS structure. This indicates that the nanocubes may be formed by the adsorption of small ZHS nanoparticles via the Oswald ripening mechanism. A similar phenomenon has been observed during synthesis of nanocube $In(OH)_3$ [24]. In order to verify this assumption, the reaction time was reduced to 10 h and a lot of small particles with irregular shape had been indeed observed (Fig. S1, Supporting information).

Fig. 6 shows the variation of benzene concentration and the concentration of the CO_2 produced over ZHS and P25 as a function of irradiation time. It shows that the initial concentration of benzene for P25 is ~234 ppm and, after turning on the lamps, the concentration decreases to about 214 ppm. Meanwhile, the concentration of CO_2 increases from 0 to 37 ppm in the initial 1 h and then quickly decreases to ~14 ppm after 5 h of operation. After 50 h of operation, the white P25 turned yellow–brown (as shown in the insert of Fig. 7) due to the deposition of reaction intermediates, leading to the deactivation of TiO_2. This is consistent with the previous observation that the TiO_2 photocatalyst is deactivated during the treatment of benzene when the feed gas does not contain sufficient H_2O [25]. For ZHS, however, the benzene concentration decreases from 252 to ~208 ppm (44 ppm benzene was converted) and a high concentration of CO_2 (~227 ppm) is steadily produced from the photooxidation of benzene, corresponding to a high benzene mineralization ratio ($[CO_2]_{produced}/[C_6H_6]_{converted}$) of 5.16. Such a high mineralization ratio suggests that about 86% of converted-benzene is completely mineralized to CO_2 and H_2O. The other 14% of converted-benzene may be degraded to some incompletely mineralized compounds, such as CO, acetaldehyde, and formaldehyde, which had been detected in our former works [13,26]. Although the benzene conversion ($[C_6H_6]_{converted}/[C_6H_6]_{initial}$) of ZHS is 17% which is smaller than that of our previously reported photocatalysts (except for InOOH), the mineralization of ZHS (86%) is substantially larger than most of them (Table 1). The high mineralization power of ZHS can effectively avoid secondary pollution during the photoreaction. In addition, compared with the high cost of In, Ga, and Ge, the low cost of ZHS make it more realistic for actual application.

The high photoactivity of ZHS can be maintained for more than 50 h, during which time no noticeable deactivation is observed. Unlike P25, the color of ZHS does not displace any apparent changes after prolonged reaction of 50 h (as shown in the insert of Fig. 7). XRD and FTIR analyses (Figs. S2 and S3, Supporting information) also show that there is no observable structural

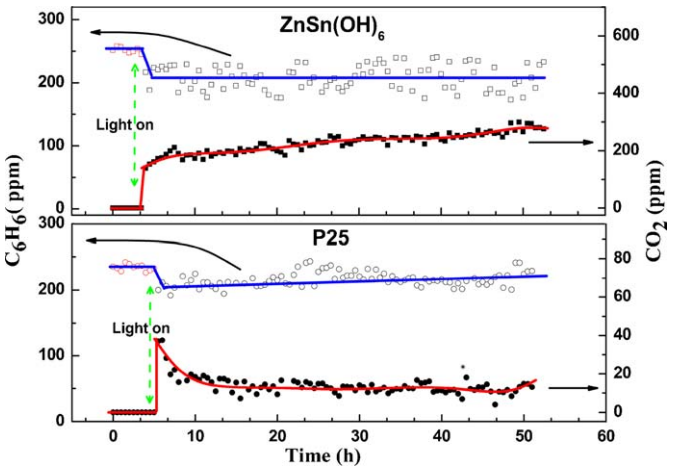

Fig. 6. The variation of benzene concentration and the amount of the CO_2 produced over $ZnSn(OH)_6$ and P25 as a function of irradiation time under UV illumination (λ = 254 nm).

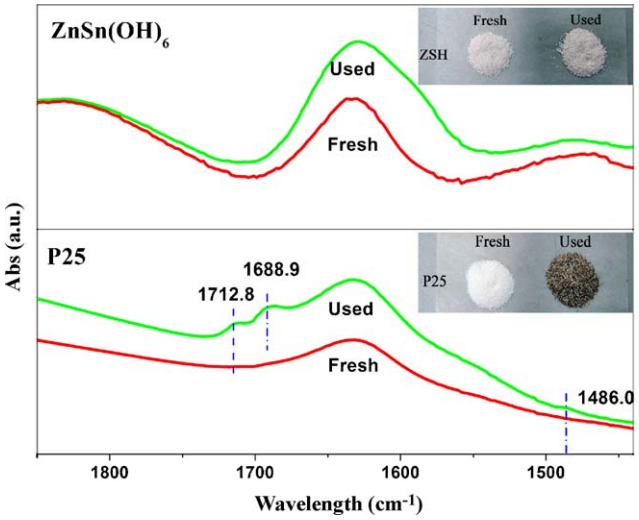

Fig. 7. FTIR spectra of fresh and used P25 and $ZnSn(OH)_6$. Insert shows the color of the fresh and used P25 and $ZnSn(OH)_6$ samples.

difference between the fresh and used ZHS. The deactivation of the P25 photocatalyst is due to the blockage of photocatalytic active sites by stable intermediates on the surface of TiO_2 during the reaction [29]. The presence of these intermediates is confirmed by FTIR analysis. As Fig. 7 shows a small band at 1486 cm^{-1}, assignable to aromatic ring C=C stretching vibration [30], reveals the deposition of some aromatic compounds on the surface of the used P25. Two bands at 1688.9 and 1712.8 cm^{-1} are assigned to C=O stretchings [6], suggesting that attack by the oxygen species upon the deposits also occurs. In contrast, for ZHS, the used sample presents a virtually identical FTIR spectrum as the fresh one without giving characteristic bands corresponding to carbonaceous materials. This indicates that no detectable reaction intermediates deposit onto the surface of ZHS during the photocatalytic

Table 1
Comparison of the conversion and mineralization efficiencies of ZHS with our former reported photocatalysts.

	$In(OH)_3$ [12]	Zn_2GeO_4 [26]	Ga_2O_3 [27]	$Sr_2Sb_2O_7$ [28]	InOOH [13]	ZHS
Conversion (%)	33.4	21	42	24	7.5	17
Mineralization (%)	52	75	95	50	52	86
V_m (μmol g^{-1} h^{-1})[a]	24.2	8.44	32.1	4.71	2.09	8.7

[a] The mineralization rate of benzene (calculated according to the reported data).

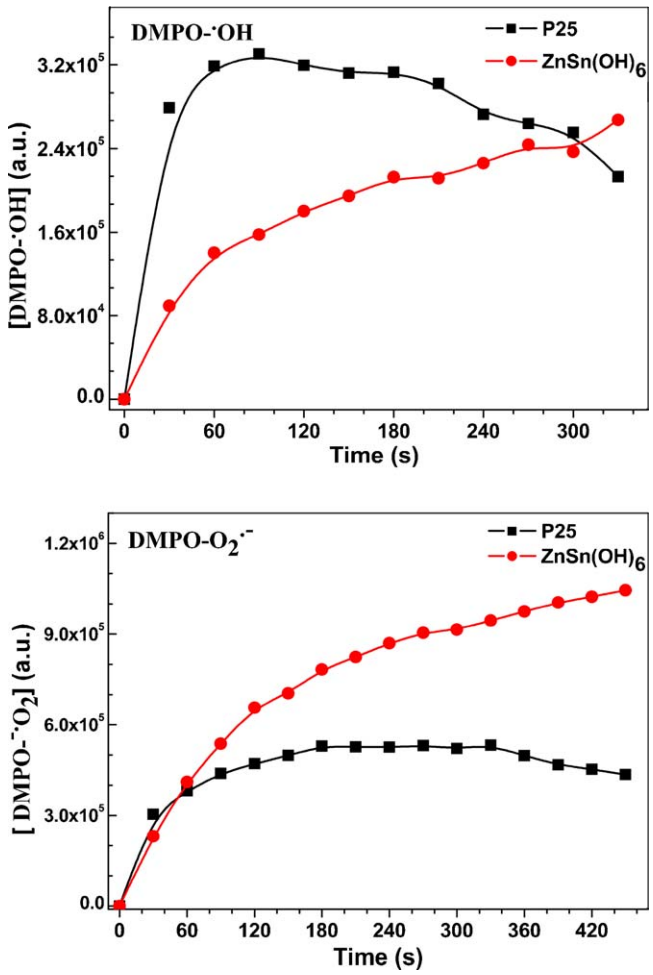

Fig. 8. Relative increase of (a) DMPO-•OH and (b) DMPO-$O_2^{\bullet-}$ concentration of P25 and $ZnSn(OH)_6$ as a function of exposure time. (In aqueous dispersion for DMPO-•OH and in methanol dispersion for DMPO-$O_2^{\bullet-}$, [DMPO] = 0.10 M, $m_{P25/ZHS}$ = 2.5 mg, $V_{solvent}$ = 0.5 mL, and wavelength of excitation = 254 nm.)

degradation of benzene, accounting for the unchanged color of ZHS.

Hydroxyl radicals (•OH) and superoxide anion radicals ($O_2^{\bullet-}$) are commonly suggested as the primary oxidizing species in the photocatalytic oxidation processes. Both for P25 and ZHS, the generation of •OH and $O_2^{\bullet-}$ radicals is confirmed by the ESR spin-trap with DMPO technique. As shown in Fig. S4 (Supporting information), when illuminated with the spot light, four characteristic peaks of DMPO-•OH with intensity of 1:2:2:1 can be obviously observed in water suspension, while six characteristic peaks of DMPO-$O_2^{\bullet-}$ adduct are observed in methanol dispersions. Similar phenomena have been reported by Liu et al. [31]. No signals can be detected without irradiation. However, for P25 and ZHS, the signal intensities of these radicals (both DMPO-•OH and DMPO-$O_2^{\bullet-}$) are clearly different with prolonged irradiation time. As Fig. 8a shows, for P25, the intensities of DMPO-•OH signals increase with the irradiation time and achieve a steady state at 60 s of irradiation, indicating an equilibrium between the production and the extinction of radicals' adducts, but about 120 s later, an initial decay of the signals is observed. Although the signal intensities of ZHS are lower than that of P25 in the early stage of illumination, they always increase with the irradiation time and no tendency to decay is observed. 300 s later, the DMPO-•OH signal intensities of ZHS are greater than those of P25. The variation tendencies of DMPO-$O_2^{\bullet-}$ signals of P25 and ZHS are similar to the changes of their DMPO-•OH signals, except that the signal intensities (DMPO-$O_2^{\bullet-}$) of ZHS are apparently larger than those of P25 (Fig. 8b).

The •OH and $O_2^{\bullet-}$ radicals are originated from the reaction of photogenerated holes (h_{vb}^+) with surface OH groups and the reaction of photoinduced electrons (e_{cb}^-) with the absorbed O_2, respectively

$$h\nu + \text{photocatalyst} \rightarrow \text{photocatalyst}\,(e_{CB}^- + h_{VB}^+)$$

$$h_{VB}^+ + \{>\text{M-OH}\} \rightarrow {}^\bullet\text{OH} + \{>\text{M}\}^+ \qquad (\text{M} = \text{Ti, ZnorSn})$$

$$e_{CB}^- + O_2 \rightarrow O_2^{\bullet-}$$

With illumination being prolonged, the OH groups of P25 are consumed in the photoreaction. Meanwhile, the dissociation of adsorbed water on the P25 surface restores the OH groups. But if the regeneration efficiency is not high enough to compensate for the consumption of OH groups, the surface OH population will be reduced, consequently decreasing the amount of •OH radicals. This may be the reason for the decay of the DMPO-OH signals of P25. However, because ZHS is a hydroxyl compound and contains hydroxyl groups as part of its lattice [14], the population of OH groups on its surface is much larger than that of P25. Thus, during the photoreaction, the density of OH groups on the ZHS surface is not as vulnerable as that of P25. Furthermore, the regeneration efficiency of OH groups of ZHS may also be greater than that of P25 and high enough to compensate for the consumption. This assumption is based on the following two factors. First, because ZHS contains hydroxyl groups as part of its lattice, compared with P25, H_2O will not only be absorbed by the ZHS surface, but also into the crystal structure [19], which increases the probability of water absorption. This characteristic is extremely important for a gas phase photocatalytic reaction causing the water is usually deficient. Second, it has been indicated that $O_2^{\bullet-}$ participates in the regeneration of OH groups [32–34]. The high efficiency of the $O_2^{\bullet-}$ formation on ZHS (as shown in Fig. 8b) will accelerate the dissociation behavior of H_2O to generate OH groups and H_2O_2.

$$\{>\text{M}\}^+ + H_2O + O_2^{\bullet-} \rightarrow \{>\text{M}-\text{OH}\} + HO_2^\bullet$$

$$HO_2^\bullet + HO_2^\bullet \rightarrow O_2 + H_2O_2$$

As a result, the surface OH groups of ZHS are recycled. H_2O_2 can be further dissociated under UV radiation [35] or reduced by photoinduced electrons [31], resulting in the promoted formation of •OH radicals.

$$H_2O_2 + h\nu \rightarrow 2{}^\bullet\text{OH}$$

or

$$H_2O_2 + e_{CB}^- \rightarrow {}^\bullet\text{OH} + OH^-$$

It is generally believed that the photocatalytic degradation of benzene proceeds via two routes [36], the direct hole oxidation or the •OH radicals oxidation. The direct hole oxidation route would produce benzene radical cations, which might react with an incoming benzene molecule resulting in the polymerization of benzene on the surface of catalysts [29]. On the contrary, this polymerization of benzene can be significantly inhibited via the •OH route. For P25, with the depletion of OH groups, direct oxidation of holes with benzene can occur. The photocatalytic activity is subsequently destroyed by the accumulation of polymerized byproducts. The FTIR data and color change of P25 (Fig. 7) confirm this reaction. However, on the ZHS surface the reaction occurred preferentially via the •OH route and the facile regeneration of OH groups further ensures the sustainability of this route. In this way, ZHS maintains a clean surface (Fig. 7) and a higher stability (Fig. 6) in the photodegradation of benzene. Although the specific process for the regeneration of OH groups,

which accounts for the catalytic recycle, is not well understood now, it can be deduced that the photocatalytic activity of benzene decomposition is highly dependent on the amount of surface OH groups. Similar phenomenon has been also observed recently by other investigators [37,38].

4. Conclusions

Cube-shaped ZHS particles have been successfully synthesized by a solvothermal process, and their photocatalytic properties were tested by a benzene oxidation reaction for the first time. The sample was found to be highly photoactive and stable toward mineralizing benzene. The high activity of ZHS was mainly attributed to the abundance of surface OH groups which accept photogenerated holes to yield highly reactive $^{\bullet}OH$ radicals. The long-term stability was ascribed to the facile regeneration of OH groups whose process involves the participation of $O_2^{\bullet-}$ and H_2O. This hydroxide may be a promising new generation of photocatalyst for benzene degradation. Further studies on the regeneration process and the photocatalytic activity of other hydroxide samples such as $BaSn(OH)_6$, $CaSn(OH)_6$, $MgSn(OH)_6$, $FeSn(OH)_6$, $MnSn(OH)_6$, and $CoSn(OH)_6$ are currently being explored in our lab.

Acknowledgments

This work is financially supported by the National Natural Science Foundation of China (Grant Nos. 20537010, 20673020, and 20873022), 863 Specialize Program (2008AA06Z326), and the National Basic Research Program of China 973 Program (Grant No. 2007CB613306). Thanks program for New Century Excellent Talents in Fujian province (XSJRC2007-19).

Appendix A. Supplementary data

Supplementary data associated with this article can be found, in the online version, at doi:10.1016/j.apcatb.2009.05.007.

References

[1] EPA, Total exposure assessment methodology (TEAM) study, Report 600/6-87/002a, Environmental Protection Agency, Washington, DC, 1987.
[2] Q. Lan, L.P. Zhang, G.L. Li, R. Vermeulen, R.S. Weinberg, M. Dosemeci, S.M. Rappaport, M. Shen, B.P. Alter, Y.J. Wu, W. Kopp, S. Waidyanatha, C. Rabkin, W.H. Guo, S. Chanock, R.B. Hayes, M. Linet, S. Kim, S.N. Yin, N. Rothman, M.T. Smith, Science 306 (2004) 1774–1776.
[3] R.M. Alberici, W.E. Jardim, Appl. Catal. B Environ. 14 (1997) 55–68.
[4] M.R. Hoffmann, S.T. Martin, W.Y. Choi, D.W. Bahnemann, Chem. Rev. 95 (1995) 69–96.
[5] G. Martra, S. Coluccia, L. Marchese, V. Augugliaro, V. Loddo, L. Palmisano, M. Schiavello, in: Proceedings of the 2nd World Congress on Environmental Catalysis, Miami, Florida, 1998.
[6] H. Einaga, S. Futamura, T. Ibusuki, Phys. Chem. Chem. Phys. 1 (1999) 4903–4908.
[7] X.Z. Fu, W.A. Zeltner, M.A. Anderson, Appl. Catal. B Environ. 6 (1995) 209–224.
[8] H. Einaga, T. Ibusuki, S. Futamura, Environ. Sci. Technol. 38 (2004) 285–289.
[9] Y.L. Chen, D.Z. Li, X.C. Wang, X.X. Wang, X.Z. Fu, Chem. Commun. (2004) 2304–2305.
[10] D.Z. Li, Z.X. Chen, Y.L. Chen, W.J. Li, H.J. Huang, Y.H. He, X.Z. Fu, Environ. Sci. Technol. 42 (2008) 2130–2135.
[11] W. Zhang, X.X. Wang, X.Z. Fu, Chem. Commun. (2003) 2196–2197.
[12] T.J. Yan, J.L. Long, Y.S. Chen, X.X. Wang, D.Z. Li, X.Z. Fu, C. R. Chim. 11 (2008) 101–106.
[13] Z.H. Li, Z.P. Xie, Y.F. Zhang, L. Wu, X.X. Wang, X.Z. Fu, J. Phys. Chem. C 111 (2007) 18348–18352.
[14] H. Jena, K.V.G. Kutty, T.R.N. Kutty, Mater. Chem. Phys. 88 (2004) 167–179.
[15] A.N. Christensen, N.C. Broch, O. Heidenstam, A. Nilsson, Acta Chem. Scand. 21 (1967) 1046–1056.
[16] J.Z. Xu, C.Y. Zhang, H.Q. Qu, C.M. Tian, J. Appl. Polym. Sci. 98 (2005) 1469–1475.
[17] F. Andre, P.A. Cusack, A.W. Monk, R. Seangprasertkij, Polym. Degrad. Stab. 40 (1993) 267–273.
[18] P.R. Hornsby, P. Winter, P.A. Cusack, Polym. Degrad. Stab. 44 (1994) 177–184.
[19] L.C. Basciano, R.C. Peterson, P.L. Roeder, I. Swainson, Can. Miner. 36 (1998) 1203–1210.
[20] Z.G. Lu, Y.G. Tang, Mater. Chem. Phys. 92 (2005) 5–9.
[21] Y.J. Zhang, M. Guo, M. Zhang, C.Y. Yang, T. Ma, X.D. Wang, J. Cryst. Growth 308 (2007) 99–104.
[22] J. Zeng, M.D. Xin, K.W. Li, H. Wang, H. Yan, W.J. Zhang, J. Phys. Chem. C 112 (2008) 4159–4167.
[23] X.L. Fu, X.X. Wang, J.L. Long, Z.X. Ding, T.J. Yan, G.Y. Zhang, Z.Z. Zhang, H.X. Lin, X.Z. Fu, J. Solid State Chem. 182 (2009) 517–524.
[24] T.J. Yan, X.X. Wang, J.L. Long, P. Liu, X.L. Fu, G.Y. Zhang, X.Z. Fu, J. Colloid Interface Sci. 325 (2008) 425–431.
[25] H. Einaga, S. Futamura, T. Ibusuki, Environ. Sci. Technol. 35 (2001) 1880–1884.
[26] J.H. Huang, X.C. Wang, Y.D. Hou, X.F. Chen, L. Wu, X.Z. Fu, Environ. Sci. Technol. 42 (2008) 7387–7391.
[27] Y.D. Hou, W.C. Wang, L. Wu, Z.X. Ding, X.Z. Fu, Environ. Sci. Technol. 40 (2006) 5799–5803.
[28] H. Xue, Z.H. Li, L. Wu, Z.X. Ding, X.X. Wang, X.Z. Fu, J. Phys. Chem. C 112 (2008) 5850–5855.
[29] S. Sitkiewitz, A. Heller, New J. Chem. 20 (1996) 233–241.
[30] S.J. Zhang, Y.F. Li, D.X. Yin, X.L. Wang, X. Zhao, Y. Shao, S.Y. Yang, Eur. Polym. J. 41 (2005) 1097–1107.
[31] G.M. Liu, X.Z. Li, J.C. Zhao, S. Horikoshi, H. Hidaka, J. Mol. Catal. A Chem. 153 (2000) 221–229.
[32] J. Arana, V.M. Rodriguez Lopez, J.M. Dona Rodriguez, J.A. Herrera Melian, J. PerezPena, Catal. Today 129 (2007) 185–193.
[33] A.R. Gonzalezelipe, G. Munuera, J. Soria, J. Chem. Soc. Faraday Trans. I 75 (1979) 748–761.
[34] H. Einaga, T. Ibusuki, S. Futamura, J. Sol. Energy Trans. ASME 126 (2004) 789–793.
[35] S.R. Cater, M.I. Stefan, J.R. Bolton, A. Safarzadeh-Amiri, Environ. Sci. Technol. 34 (2000) 659–662.
[36] O. d'Hennezel, P. Pichat, D.F. Ollis, J. Photochem. Photobiol. A 118 (1998) 197–204.
[37] N. Wang, J. Li, L.H. Zhu, Y. Dong, H.Q. Tang, J. Photochem. Photobiol. A 198 (2008) 282–287.
[38] P. Du, A. Bueno-López, M. Verbaas, A.R. Almeida, M. Makkee, J.A. Moulijn, G. Mul, J. Catal. 260 (2008) 75–80.